Supplemental Figures and Movie Legend – *McClintock et al. "RNA-directed activation of cytoplasmic dynein-1 in reconstituted transport RNPs"*

Figure S1. Alignment of binding site for Rab6^{GTP} and Egl in *Drosophila melanogaster* BicD with the corresponding region of mouse and human BICD2. The *Drosophila* sequence has 71% identity and 93% similarity with the mouse and human sequence.

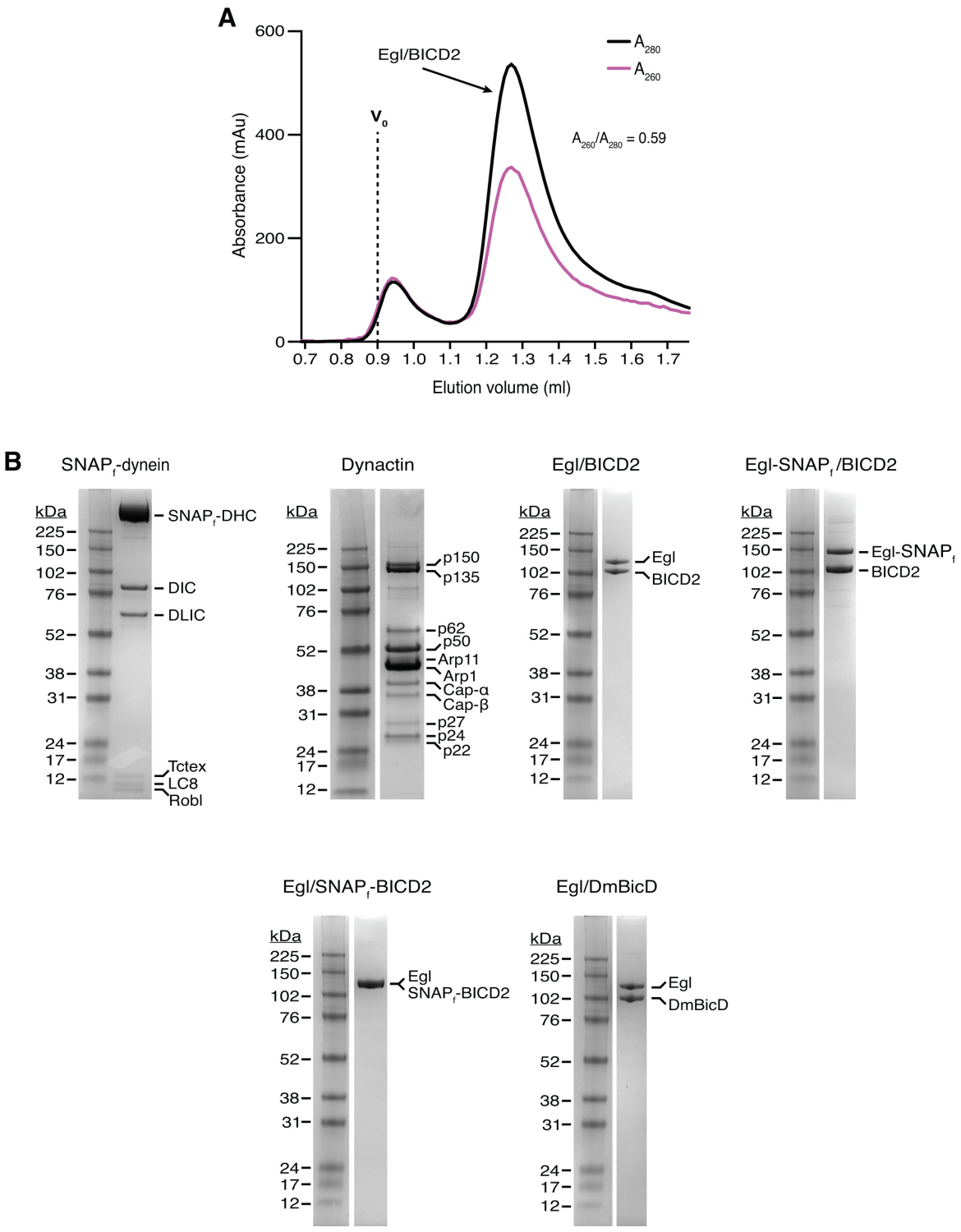

Figure S2. Purity of protein preparations. (A) Size-exclusion chromatography (SEC) trace produced in GF150 buffer at 4ºC (Superose 6 Increase 3.2/300). The ratio of absorbance values at 260 nm to 280 nm for the peak fractions indicates that there is little, if any, RNA co-purified from the insect cells (A_{260}:A_{280} is 0.57 for pure protein and 1.05 for a sample with 95% protein and 5% nucleic acid (Glasel, 1995)). V_o: void. (B) Examples of Coomassie-stained gels illustrating purity of protein preparations. Note that the native brain dynactin contains both the p150 and p135 isoforms of DCTN1/Glued, as described previously (Schlager et al, 2014).

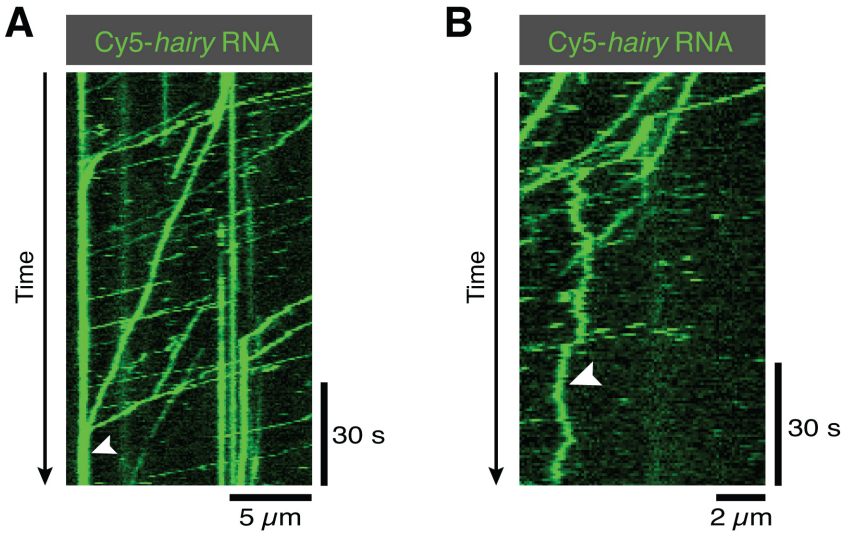

Figure S3. Additional behaviours of *hairy* RNA in the presence of Egl/BICD2, dynactin and dynein. (A) Kymograph illustrating accumulation of transported RNPs at the microtubule minus end (arrowhead). (B) Kymograph illustrating diffusive behaviour on the microtubule lattice (arrowhead).

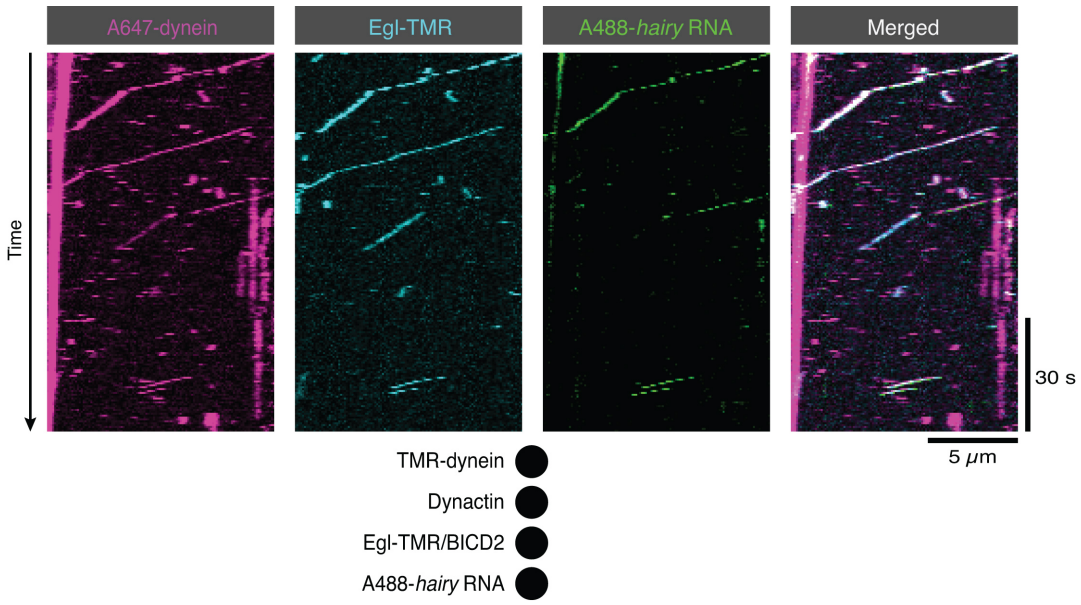

Figure S4. Co-transport of Egl with dynein and RNA in the presence of BICD2 and dynactin. Kymographs illustrating transport of dynein with Egl (included in the assay in a complex with unlabelled BICD2) and *hairy* mRNA in the presence of unlabelled dynactin. See Figure 2A for data from an analogous experiment in which BICD2 was labelled fluorescently within the Egl/BICD2 complex.

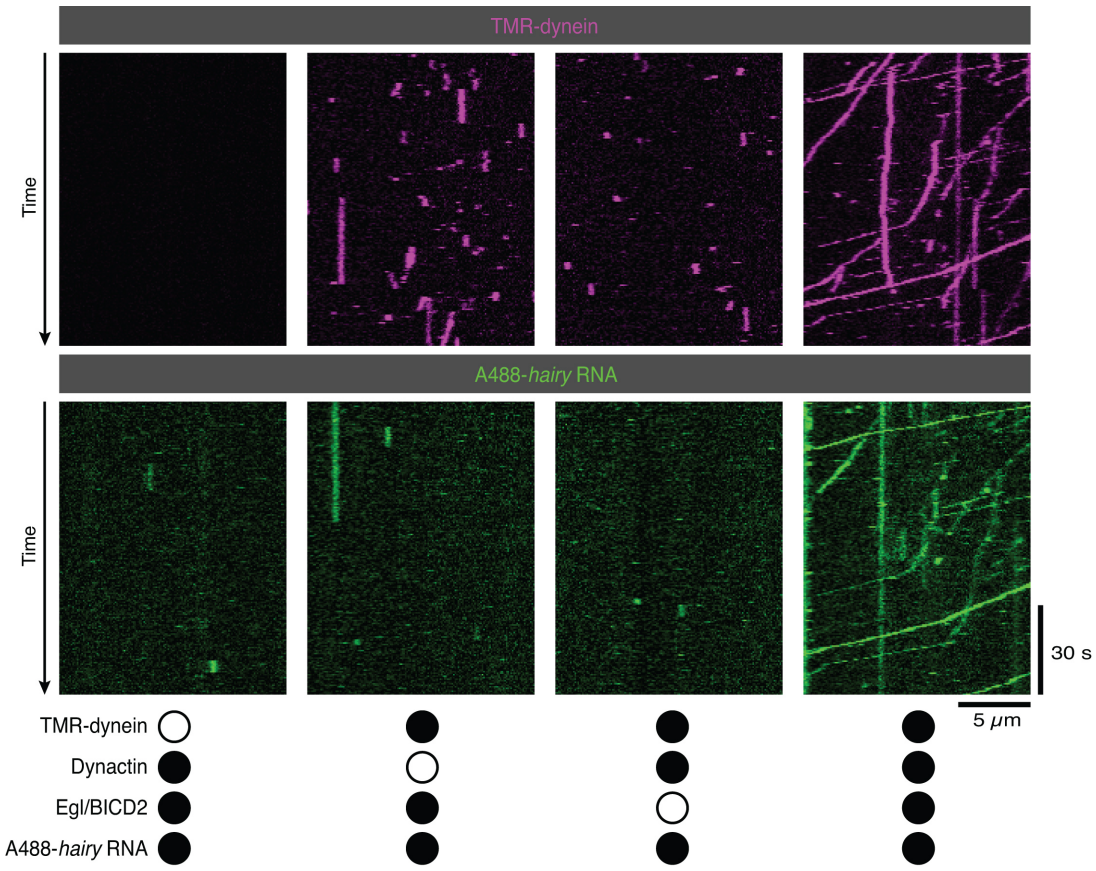

Figure S5. Supplementary data on the requirement for Egl/BICD2 and dynactin for binding of RNA to microtubules and dynein motility. Images are individual channels for the merged data in Figure 2B.

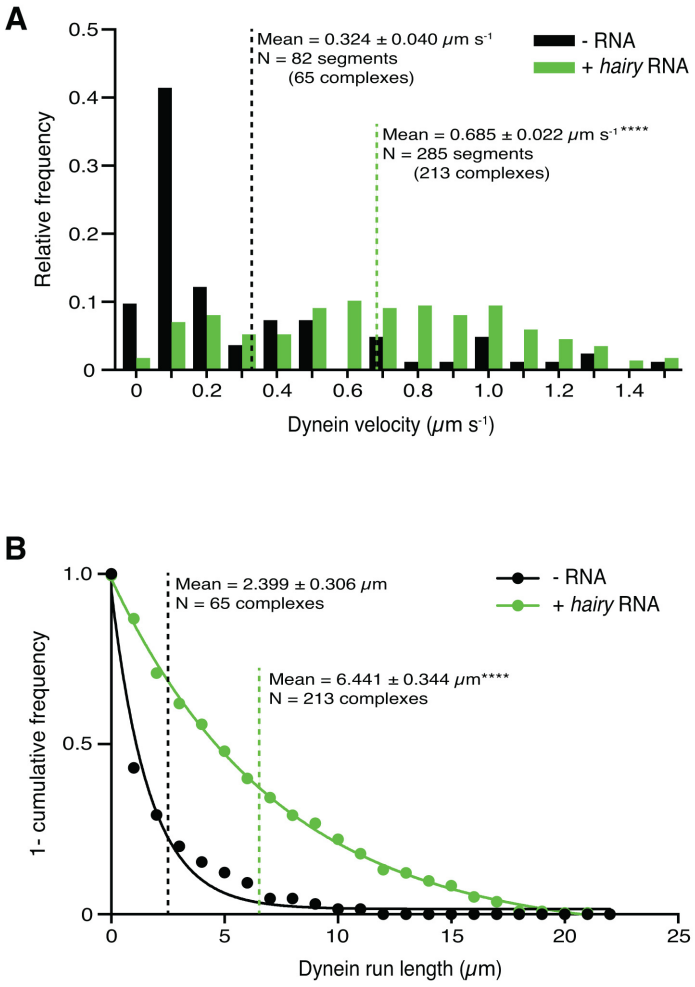

Figure S6. Supplementary data on dynein motility in the presence of dynactin, Egl/DmBicD and *hairy* RNA. (A and B) Distribution of segmental velocities (A) and run lengths (B) of dynein in the presence of Egl/DmBicD and dynactin ± *hairy* RNA. Means ± SEM are shown for the raw, unfitted values; statistical significance (compared to the equivalent parameter in the absence of RNA) was evaluated with a Mann-Whitney test. ****, P <0.0001.

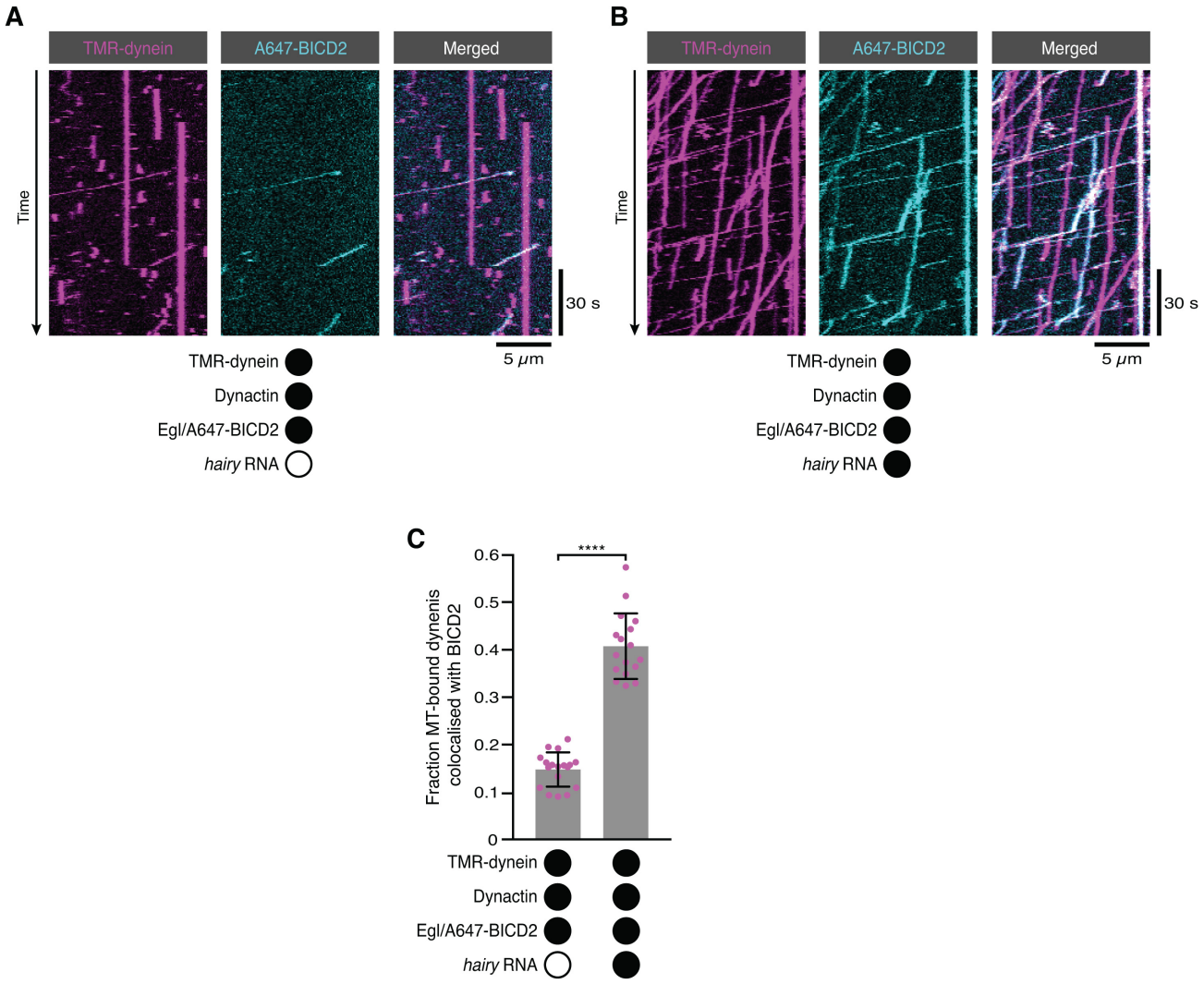

Figure S7. RNA promotes the association of BICD2 with dynein in the presence of Egl and dynactin. (A, B) Kymographs illustrating the behaviour of fluorescently-labelled versions of dynein and BICD2 (included in the assay in a complex with unlabelled Egl) in the presence of dynactin ± *hairy* RNA. (C) Fraction of microtubule-associated dyneins that associate with BICD2 in the presence of Egl/BICD2, dynactin ± *hairy* RNA. Circles are values for individual microtubules. Error bars: SD. Statistical significance was evaluated with a Welch's *t*-test. ****, P<0.0001.

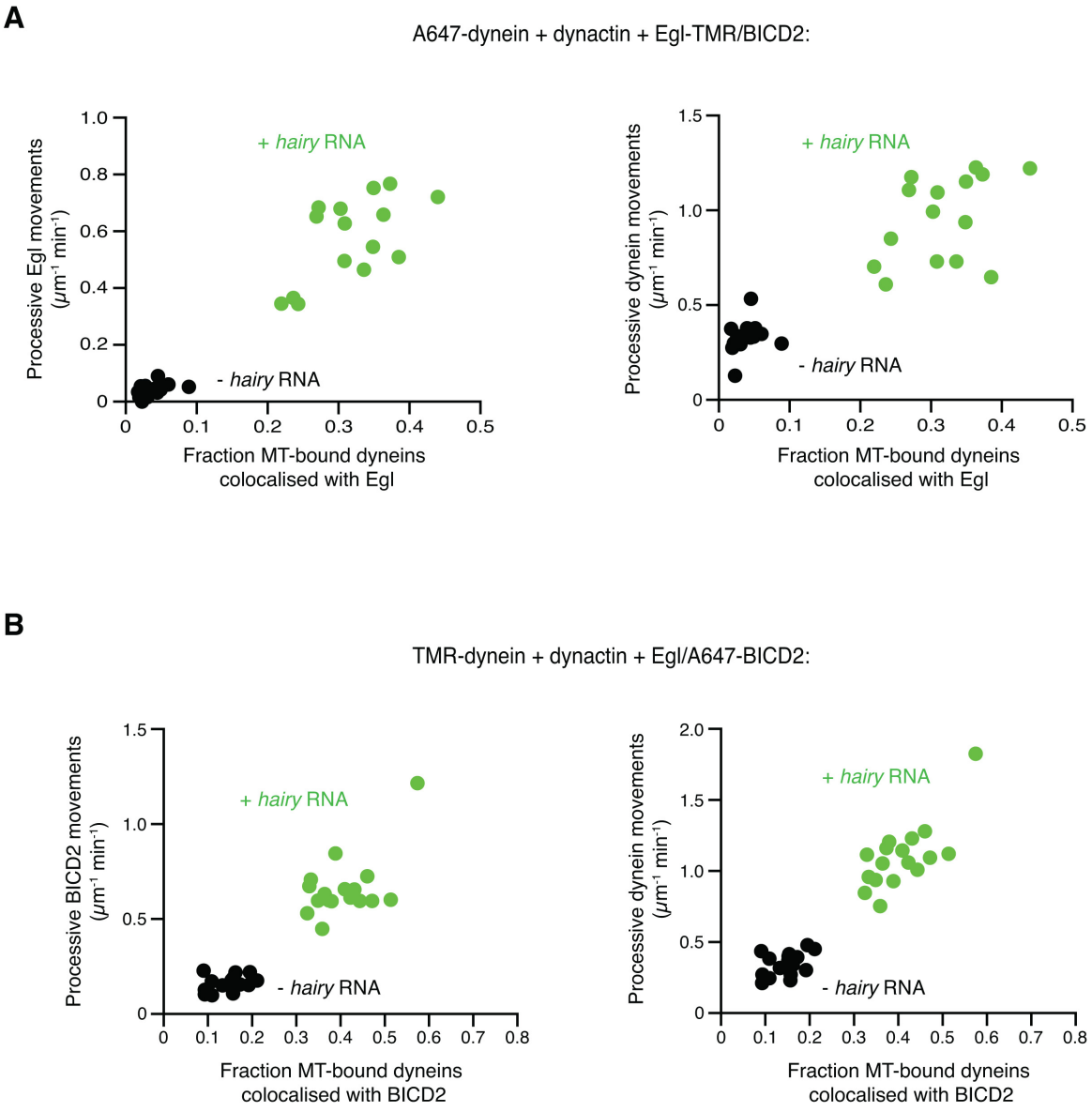

Figure S8. RNA-induced association of Egl/BICD2 with dynein promotes transport. (A, B) Correlation between co-localisation of Egl (A) or BICD2 (B) with dynein and transport (each included in the assay in the context of the Egl/BICD2 complex). Circles are values for individual microtubules.

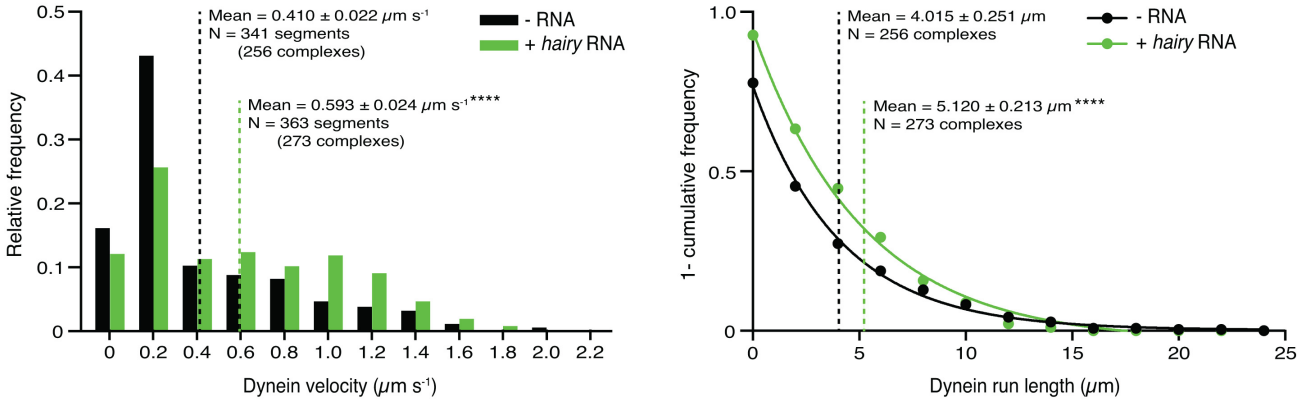

Figure S9. Supplementary data on dynein motility in the presence of dynactin, Egl^{dlc2pt}/BICD2 and *hairy* RNA. (A and B) Distribution of segmental velocities (A) and run lengths (B) of dynein in the presence of Egl^{dlc2pt}/BICD2 and dynactin ± *hairy* RNA. Means ± SEM are shown for the raw, unfitted values; statistical significance (compared to the equivalent parameter in the absence of RNA) was evaluated with a Mann-Whitney test. ****, P <0.0001.

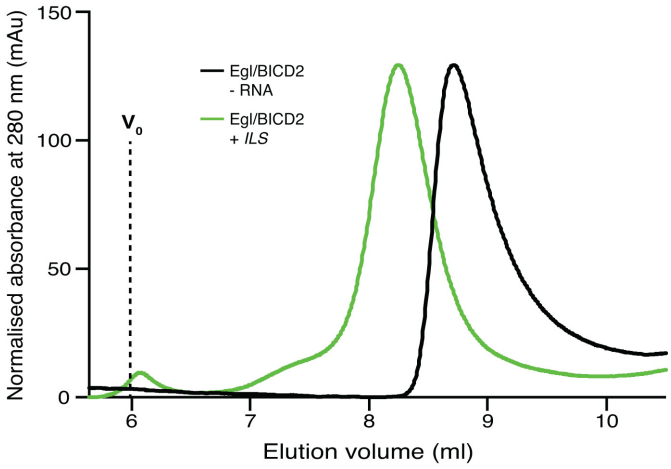

Figure S10. The *ILS* leads to a significant change in the SEC elution profile of the Egl/BICD2 complex. The purified Egl/BICD2 complex was incubated with a 10-fold molar excess of the *ILS* (assuming two Egl molecules and one BICD2 dimer per complex) and subjected to SEC (G4000SWxl with guard column) in GF150 buffer at 4ºC. V_o: void.

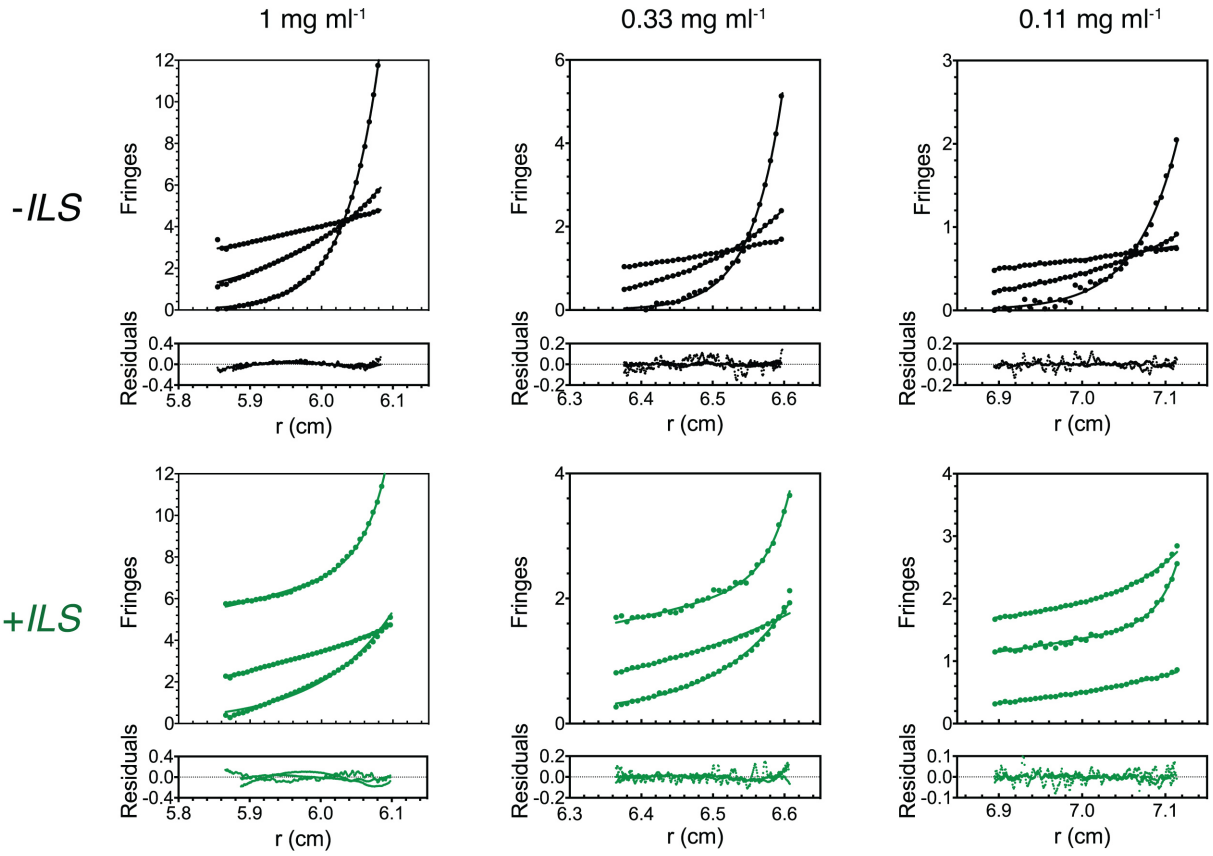

Figure S11. Supplementary data for SE-AUC analysis. Raw data and goodness of fit are shown for one sample per concentration in the presence and absence of RNA. Curves indicate data from runs at different velocities.

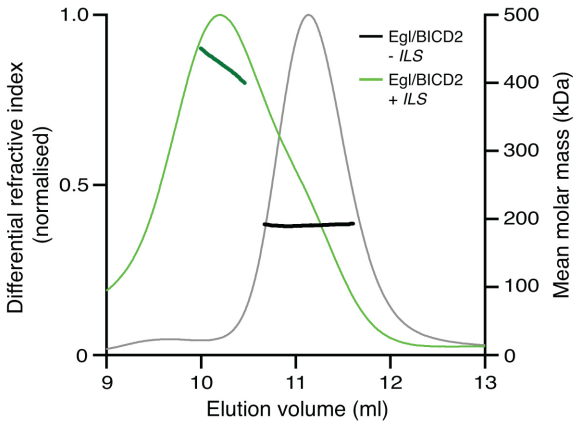

Figure S12. SEC-MALS data for the purified Egl/BICD2 complex in the presence and absence of the *ILS* using buffer with reduced salt concentration (75 mM). See Figure 6B for data obtained with a higher salt buffer (150 mM). The mean molar mass of the RNA-free sample (190.7 ± 0.2 kDa) is similar to that observed with the higher salt buffer. In the presence of the *ILS*, however, reducing salt concentration causes a significant increase in the molar masses observed. This observation suggests that the RNA-bound Egl/BICD2 complex is particularly sensitive to ionic strength. The experiment was performed at room temperature, as was the case for the experiment documented in Figure 6B.

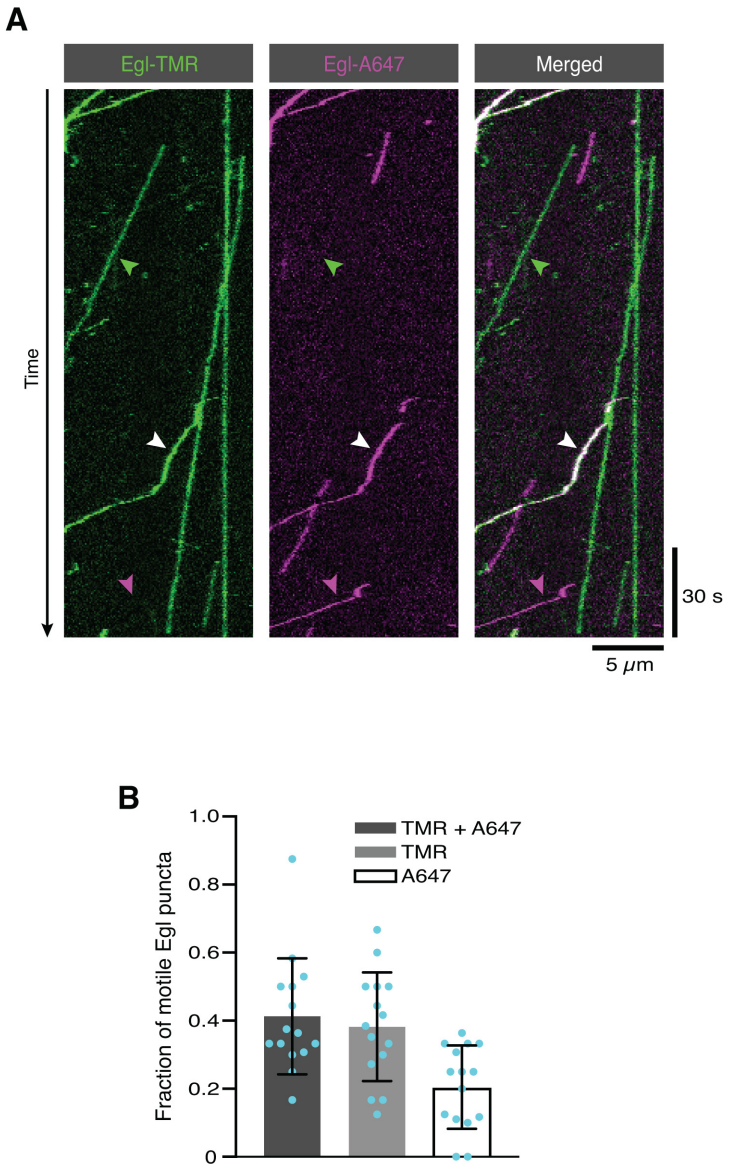

Figure S13. The presence of two Egl proteins in active transport complexes assembled in the absence of RNA. (A) Kymograph of fluorescent signals when Egl-SNAP/BICD2 is labelled with a mixture of TMR and Alexa647 and assayed in the presence of dynactin and dynein but in the absence of RNA. White, green and magenta arrowheads show, respectively, examples of motile Egl-containing complexes with signals from both fluorophores, only TMR, or only Alexa647. (B) Fraction of motile Egl-containing complexes labelled with signals from both fluorophores, only TMR, or only Alexa647. Circles are values for individual microtubules. Variance is high because of the small number of motile complexes per microtubule.

Movie Legend

Movie S1. Movements of Cy5-*hairy* RNPs (green) on surface-immobilised microtubules in the presence of Egl/BICD2, dynactin and dynein. The positions of the microtubules can be inferred by the movement of the RNPs. Width of frame is 45.15 µm; movie corresponds to 252 s of real time.

Supplemental References

Glasel JA (1995) Validity of nucleic acid purities monitored by 260nm/280nm absorbance ratios. BioTechniques 18: 62-63.

Schlager MA, Hoang HT, Urnavicius L, Bullock SL, Carter AP (2014) In vitro reconstitution of a highly processive recombinant human dynein complex. EMBO J 33: 1855-1868. doi: 10.15252/embj.201488792